THE JOURNAL OF PHYSICAL CHEMISTRY B

Article

pubs.acs.org/JPCB

Pulse Q-Band EPR and ENDOR Spectroscopies of the Photochemically Generated Monoprotonated Benzosemiquinone Radical in Frozen Alcoholic Solution

Marco Flores,*[,†,§] Melvin Y. Okamura,[‡] Jens Niklas,[†,∥] Maria-Eirini Pandelia,[†,⊥] and Wolfgang Lubitz*[,†]

[†]Max-Planck-Institut für Chemische Energiekonversion, Mülheim an der Ruhr, D-45470, Germany

[‡]Department of Physics, University of California at San Diego, La Jolla, California 92093, United States

Supporting Information

ABSTRACT: Quinones are essential cofactors in many physiological processes, among them proton-coupled electron transfer (PCET) in photosynthesis and respiration. A key intermediate in PCET is the monoprotonated semiquinone radical. In this work we produced the monoprotonated benzosemiquinone ($BQH^{\bullet}$) by UV illumination of BQ dissolved in 2-propanol at cryogenic temperatures and investigated the electronic and geometric structures of $BQH^{\bullet}$ in the solid state (80 K) using EPR and ENDOR techniques at 34 GHz. The *g*-tensor of $BQH^{\bullet}$ was found to be similar to that of the anionic semiquinone species ($BQ^{\bullet-}$) in frozen solution. The peaks present in the ENDOR spectrum of $BQH^{\bullet}$ were identified and assigned by $^{1}H/^{2}H$ substitutions. The experiments reconfirmed that the hydroxyl proton (O−H) on $BQH^{\bullet}$, which is abstracted from a solvent molecule, mainly originates from the central CH group of 2-propanol. They also showed that the protonation has a strong impact on the electron spin distribution over the quinone. This is reflected in the hyperfine couplings (hfc's) of the ring protons, which dramatically changed with respect to those typically observed for $BQ^{\bullet-}$. The hfc tensor of the O−H proton was determined by a detailed orientation-selection ENDOR study and found to be rhombic, resembling those of protons covalently bound to carbon atoms in a π-system (i.e., α-protons). It was found that the O−H bond lies in the quinone plane and is oriented along the direction of the quinone oxygen lone pair orbital. DFT calculations were performed on different structures of $BQH^{\bullet}$ coordinated by four, three, or zero 2-propanol molecules. The O−H bond length was found to be around 1.0 Å, typical for a single covalent O−H bond. Good agreement between experimental and DFT results were found. This study provides a detailed picture of the electronic and geometric structures of $BQH^{\bullet}$ and should be applicable to other naturally occurring quinones.

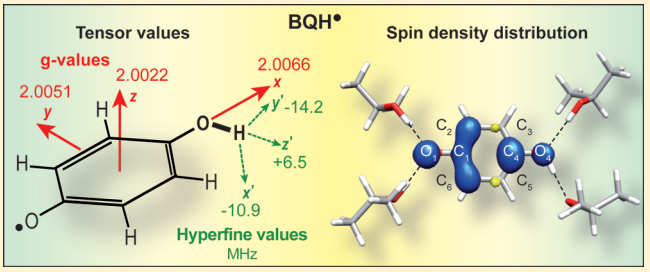

INTRODUCTION

Quinone molecules such as ubiquinone and plastoquinone play an important role as cofactors in many proteins of the mitochondrial respiratory chain and in photosynthesis.[1−5] Prominent examples of such energy conserving systems are photosynthetic reaction centers, cytochrome bc_1, and NADH ubiquinone reductase. Quinones can be fully reduced in two successive reversible single-proton-coupled electron transfer steps, $Q + 2H^{+} + 2e^{-} \rightarrow QH_2$.[1,6] The first step involves two paramagnetic intermediates, the semiquinone radical anion $Q^{\bullet-}$ and the neutral monoprotonated semiquinone radical $QH^{\bullet}$; the second step leads to the fully reduced quinol. As a result of this versatile behavior, quinones are involved in many biological electron transfer reactions and in proton translocation across membranes, two important processes occurring in respiration and photosynthesis.[4] The semiquinone radical anion is the most commonly observed form of the semiquinone in biological systems[7−10] due to the low pK_a of the monoprotonated semiquinone radical. However, the protonated semiquinone is also involved in quinone reactions. It has been proposed as an intermediate in bacterial reaction centers,[11] cytochrome bc_1,[12] and cytochrome bo_3 ubiquinol oxidase,[13,14] where the protonation and deprotonation reactions play important roles in proton transfer across the membrane.

A variety of spectroscopic methods including electron paramagnetic resonance (EPR) and electron−nuclear double resonance (ENDOR) spectroscopies have been extensively used to investigate the semiquinone radical anion.[15−26] However, far less information is available for protonated semiquinones due to their rapid dismutation. To study the protonated semiquinone radical outside the protein, it can be formed by UV illumination of the respective quinone in alcohol solution.[27,28] Under these conditions, the protonated semiquinone is most likely formed by hydrogen atom abstraction from an adjacent solvent molecule.[29] An alternative mechanism involving electron transfer followed by proton binding has also

Received: May 10, 2012
Revised: June 25, 2012
Published: June 25, 2012

been proposed.[30] The protonated semiquinone formed by UV illumination has previously been trapped at cryogenic temperature and studied by EPR and infrared spectroscopy.[31,32] Some information on protonated semiquinone radicals is available from previous EPR[28,31,33,34] and ENDOR[35] work, but our knowledge about the properties of the hydroxyl proton (O−H) of the monoprotonated semiquinone is still incomplete. The O−H is a unique feature of the protonated semiquinone radical; therefore, its geometry and magnetic properties must be characterized. Such properties could be useful for the identification of protonated semiquinone species in biological systems. In this work, we present a Q-band EPR and ENDOR study on the protonated 1,4-benzosemiquinone radical produced by illumination of the quinone in 2-propanol at cryogenic temperatures. The monoprotonated species can be generated with sufficiently high yield and purity and is an excellent model for other more complicated quinones occurring in nature, like ubiquinone and plastoquinone. All experiments were done at a microwave frequency of 34 GHz (Q-band) that, compared to the commonly used 9 GHz (X-band), provides improved spectral resolution, enabling the selection of molecules with particular orientations with respect to the magnetic field.[36−38] The source of the proton bound by the quinone oxygen was determined by isotope substitution (H/D) experiments. In addition, from analysis of the orientation selected ENDOR spectra, the hyperfine coupling tensor of the hydroxyl was determined. On the basis of the magnetic parameters, the geometry of the bound proton could be elucidated.

The structure of the radical and its magnetic properties were calculated using density functional theory (DFT),[39,40] a method that has proven to successfully predict the electronic and geometric structures of (H-bonded) quinone radicals in frozen organic solvents and biological systems.[41−45]

THEORY

Spin Hamiltonian. The systems studied in this work are frozen alcoholic solutions of the monoprotonated 1,4-benzosemiquinone radical shown in Figure 1. We focus on the interaction between the magnetic moment of the unpaired electron of the radical ($BQH^{\bullet}$) and the magnetic moments of protons bound to the quinone (see Figure 1). The observed ENDOR spectra are interpreted using a spin Hamiltonian, $\mathcal{H}$, containing the electron and nuclear Zeeman interactions and the hyperfine coupling (hfc) terms:[46]

$$\mathcal{H} = \beta_e \mathbf{S}\cdot\mathbf{g}\cdot\mathbf{B_o} - \beta_N g_N \mathbf{I}\cdot\mathbf{B_o} + h\mathbf{S}\cdot\mathbf{A}\cdot\mathbf{I} \quad (1)$$

where $\mathbf{B_o}$ is the applied magnetic field, $\mathbf{S}$ is the electron spin operator, $\mathbf{I}$ is the nuclear spin operator of either a proton covalently bound to the quinone ring or the proton that binds to one of the carbonyl oxygens, $\mathbf{A}$ is the hfc tensor in frequency units, $\mathbf{g}$ is the electronic g-tensor, g_N is the nuclear g factor of the proton, β_e and β_N are the electron and nuclear magnetons, respectively, and h is Planck's constant. The first term in eq 1 represents the electronic Zeeman interaction that gives rise to the observed EPR spectra. This interaction is anisotropic and depends on the relative orientation between the magnetic field and the molecular axes of the quinone. The other two terms represent nuclear interactions, which are small and often not resolved in the EPR spectrum but may be resolved in the ENDOR spectra. To first order, the positions of the ENDOR lines can be written as[46,47]

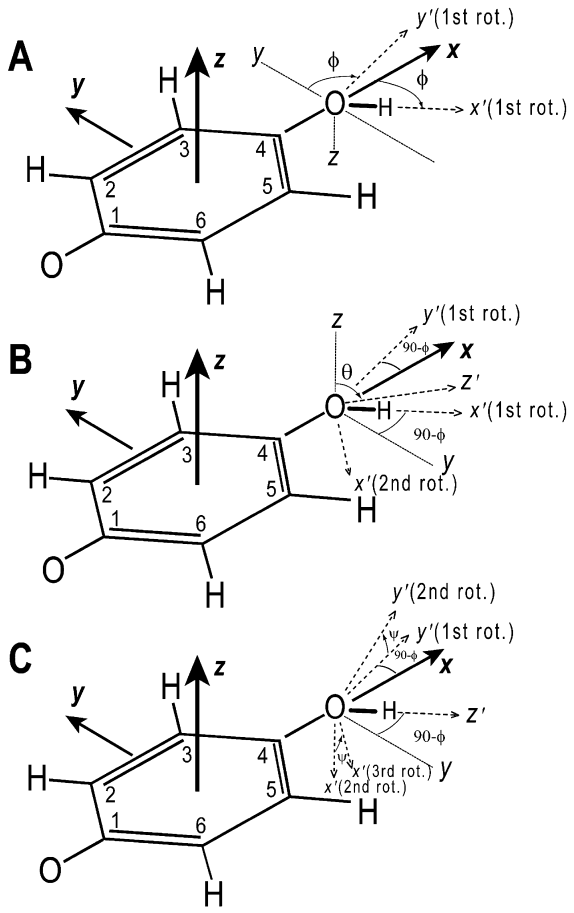

Figure 1. Molecular structure of the monoprotonated benzosemiquinone radical ($BQH^{\bullet}$). The principal axes of the g-tensor are expected to be approximately along the molecular axes x, y, and z (see the DFT section). The principal axes of the hfc tensor corresponding to the O−H proton are along the axes x', y', and z', which are related to the g-tensor axes by rotations: (A) around z (angle ϕ) followed by consecutive rotations (B) around y' (angle θ) and (C) around z' (angle ψ).[53] The first two Euler angles, ϕ and θ, define the direction of the O−H bond (B). The rotation around z' (angle ψ) is shown for the case in which the O−H proton lies in the plane of the quinone (θ = 90°) (C).

$$\nu_{ENDOR} = |AM_S - g_N\beta_N B_o/h| \quad (2)$$

where M_S is the magnetic quantum number of the unpaired electron (±1/2). Thus, for a given magnetic field direction with respect to the molecular axes, one expects two ENDOR lines separated by the hfc A centered around the proton Larmor frequency $g_N\beta_N B_o/h$. In a sample with randomly oriented molecules (powder or frozen solutions), the anisotropy of A smears out over the entire spectral range and sharp lines are observed only at the extrema (e.g., A_x, A_y, and A_z).

The hfc tensor component A_i is composed of anisotropic and isotropic contributions that can be written as

$$A_i = A_i' + A_{iso} \quad (3)$$

The anisotropic part, arising from the dipolar interaction between the unpaired electron and the proton, provides information on the geometry (i.e., position and direction) of the proton relative to the molecule, and the isotropic part gives information about the wave function of the unpaired electron at the proton position. A larger interaction means most likely a

dx.doi.org/10.1021/jp304555u | J. Phys. Chem. B 2012, 116, 8890−8900

smaller distance between the proton and the unpaired electron spin. For the monoprotonated 1,4-benzosemiquinone radical, three different types of protons are expected:

(a) Protons in hydrogen bonds: For this kind of protons, the isotropic part A_{iso} is small compared to the anisotropic term A_i' (eq 3).[23,42,48,49] The hyperfine coupling tensor is nearly axially symmetric with the symmetry axis along the hydrogen bond direction. The strength of the interaction is proportional to the hydrogen bond length (strength).[23,43]

(b) Ring (α) protons: In this case, the hyperfine coupling tensors (eq 3) are usually rhombic; the large isotropic component reflects the spin density at the neighboring C(π)-atom.[50] Note that in the case of a large spin density at close-by non-neighboring atoms, e.g., the carbonyl group in quinone radicals, nearly axially symmetric proton hyperfine tensors have been reported with the symmetry axis close to the direction of the molecular y-axis.[51,52]

(c) The O−H proton: The magnetic resonance properties of this kind of proton are not fully characterized yet and are the main subject of this study. However, the hyperfine coupling tensor of the O−H proton is expected to be rhombic.

Molecular Structure and Axis System. Since the hfc tensor axes are not expected to be collinear with the g-tensor axes of the monoprotonated semiquinone radical ($BQH^{\bullet}$),[46,50] we describe this tensor by its principal components and the Euler angles[53] thereby relating its principal axes to the g-tensor axes (see Figure 1). Furthermore, the hfc tensor of the O−H proton is expected to have rhombic symmetry.[50] In this work, we used frozen solutions at 80 K containing randomly oriented molecules. ENDOR spectra were obtained at different magnetic field positions within the EPR spectrum, along which molecules with a particular set of directions were selected.[36−38,53] The global analysis by computer simulations of the ENDOR spectra,[37,38] using the spin Hamiltonian of eq 1, yielded both the principal components of the hyperfine coupling tensor and its orientation (i.e., Euler angles) with respect to the principal axes of the g-tensor of $BQH^{\bullet}$.

The monoprotonated benzosemiquinone ($BQH^{\bullet}$) molecule is shown in Figure 1. The principal axes of the g-tensor are expected to be approximately parallel to the molecular axes x, y, and z, with the z-axis perpendicular to the π-plane. This assumption is supported by the DFT calculations performed in this work (see the DFT section). The principal axes of the hfc tensor of the O−H proton are denoted by x', y', and z', with z' (axis defined by the two first Euler rotations) corresponding to the smallest component of the hfc tensor. The largest component of the hfc tensor is along the y' axis. Figure 1 also shows the Euler angles (ϕ, θ, ψ) relating the x', y', and z' axes to the g-tensor axes.[53]

MATERIALS AND METHODS

Sample Preparation. Benzoquinone (BQ) was obtained from Aldrich (Milwaukee, WI) and purified by vacuum sublimation. The fully deuterated benzoquinone (BQ-d_4) was prepared as described by Zhao et al.[54] The degree of deuteration was 96 ± 2%, as determined by mass spectrometry. The deuterated alcohols were obtained from Aldrich (Milwaukee, WI). Solvents were distilled on a vacuum line prior to sample preparation.

BQ was dissolved in differently protonated/deuterated deoxygenated 2-propanol (conc. ∼3 mM). The sample was transferred to a quartz tube (OD 3 mm, ID 2 mm) under argon (99.99%) and subsequently sealed. The sample was frozen in liquid nitrogen and placed in a quartz dewar cooled with liquid nitrogen. The monoprotonated benzosemiquinone radical ($BQH^{\bullet}$) was generated by illumination with an HBO 200W/2 xenon light source (Lot-Oriel), $I \sim 800$ mW/cm^2, for 30 min. Subsequently, the sample was quickly transferred to the spectrometer without thawing.

The benzoquinone radical anion ($BQ^{\bullet-}$) was generated using procedures described elsewhere.[42,48] BQ was dissolved in fully deuterated deoxygenated 2-propanol (conc. ∼1 mM). To the deoxygenated solution, 0.1 M benzyl trimethylammonium hydroxide was added as a base together with a trace of benzoin, which serves as a reductant. The sample was transferred to a quartz tube (OD 3 mm, ID 2 mm) under argon (99.99%) and frozen by plunging it into liquid nitrogen.

EPR and ENDOR Instrumentation. Pulsed Q-band (34 GHz) EPR and ENDOR measurements were performed on a Bruker ELEXSYS E580 spectrometer with a Super Q-FT Microwave Bridge equipped with a home-built resonator[55] that allows large sample tubes with OD = 3 mm. The magnetic field was calibrated using a Mn^{2+} powder sample (0.02% in MgO) as a g-value standard (g = 2.00101).[56] Field-swept free induction decay (FID)-detected EPR spectra were recorded using a hole-burning microwave (MW) pulse of 1000 ns. Field-swept electron spin echo-detected EPR spectra were recorded using the two-pulse echo sequence ($\pi/2-\tau-\pi-\tau-$echo). Microwave (MW) pulses of 40 ns ($\pi/2$) and 80 ns (π) and τ = 340 ns were used. ^{1}H ENDOR spectra were recorded using the Davies ENDOR sequence[57] ($\pi-t-\pi/2-\tau-\pi-\tau-$echo) with a MW inversion π-pulse of 300 ns, t = 21 μs, radio frequency (RF) π-pulse of 18 μs, and a detection sequence similar to that of the echo-detected EPR experiment. An ENI 3200 L (300 W) RF amplifier was used for ^{1}H ENDOR measurements. All experiments were performed at T = 80 K, using an Oxford CF935 cryostat.

Simulation of Spectra. EPR and ENDOR spectra were fitted using EasySpin (v 3.0.0), a computational package developed by Stoll and Schweiger[58] and based on Matlab (The Mathworks, Natick, MA, USA). The EPR fitting procedure used a Monte Carlo type iteration to minimize the root-mean-square deviation, σ (see eq 1 of the Supporting Information) between measured and simulated spectra. We searched for the optimum values of the parameters g_x, g_y, and g_z and the line widths ΔB_x, ΔB_y, and ΔB_z.

ENDOR frequencies were calculated using the energies of the states of the spin system obtained by direct diagonalization of the spin Hamiltonian (see eq 1). Two sets of parameters were used in the ENDOR simulations. The first set includes the EPR parameters, i.e., the microwave frequency, g-values (obtained from the fitting of the EPR spectrum), and magnetic field position. These parameters remained fixed in the ENDOR simulations. The second set consists of the following fitting parameters: the principal values and Euler angles of the hyperfine coupling tensor ($A_{x'}$, $A_{y'}$, $A_{z'}$, ϕ, θ, ψ), the excitation width (Δw_k) (i.e., the EPR line width at the magnetic field position of the ENDOR measurement), and the ENDOR line width ($\Delta \nu_k$). These parameters were varied iteratively, one at a time, to simultaneously optimize the fit of the ENDOR spectra at different positions of the EPR spectrum by minimizing the value of σ_G (global fitting, see eq 2 of the Supporting

Information). The process was terminated when no further changes in the values of the fitting parameters were observed. This required typically four iterations over the full set of fitting parameters.

Density Functional Theory Calculations. Density functional theory calculations were performed on the monoprotonated benzosemiquinone ($BQH^{\bullet}$) molecule with zero, three, or four hydrogen bonds to the radical. The B3LYP density functional[39,59−61] and DZPD basis set[62,63] were used for geometry optimizations. The geometry optimizations were performed with ORCA (v 2.9)[64] without any constraints and employing the conductor screening model (COSMO), to ensure that the optimized geometries reflect the approximate effects of the environment of the molecule.[65,66] In the present study, a dielectric constant of $\varepsilon = 20.18$ was used considering 2-propanol molecules as the solvent. Single-point calculations, *g*-tensors, and hyperfine parameters were calculated using the B3LYP density functional and the EPR II basis set[67] also employing the conductor-like screening model with $\varepsilon = 20.18$.

RESULTS AND DISCUSSION

EPR Experiments. By illuminating 1,4-benzoquinone in $(CH_3)_2CHOH$ at 77 K (see Materials and Methods), EPR signals corresponding to two different paramagnetic species were observed. One corresponds to the monoprotonated benzosemiquinone radical ($BQH^{\bullet}$-h_4) and the other to the solvent radical ($(CH_3)_2C^{\bullet}OH$).[29,68] These assignments were confirmed by the ENDOR spectra. The ENDOR experiments showed that also the benzoquinone radical anion ($BQ^{\bullet-}$) was created with low yield (see below). The $BQ^{\bullet-}$ may be formed from secondary chemical events, like the deprotonation of the semiquinone[69] or an electron-transfer reaction from the hydroxyalkyl radical to benzoquinone as in the case of duroquinone.[70] Thus, this paramagnetic species is supposed to give only a minor contribution to the EPR spectrum. The signals increased in amplitude with illumination time and reached their maximum amplitude in about 30 min. The EPR signals of $BQH^{\bullet}$-h_4 and $(CH_3)_2C^{\bullet}OH$ overlap (see Figure S1 of the Supporting Information).[68] However, they showed characteristics, e.g., line width and relaxation times, of individual radicals, reflecting a negligible magnetic interaction between the two paramagnetic species.

Figure 2 (solid line) shows the Q-band EPR spectrum of the monoprotonated benzosemiquinone radical using fully deuterated benzoquinone ($BQH^{\bullet}$-d_4) in $(CH_3)_2CHOD$. As a consequence of the smaller magnetic moment of the deuteron, the hyperfine splittings of the ring deuterons are not resolved in the spectrum (see Figure 2), allowing a more accurate determination of the *g*-values corresponding to the radical (see Table 1). To obtain orientation selection, ^{1}H ENDOR spectra were recorded at the magnetic field positions B_i indicated by arrows in Figure 2.

ENDOR Experiments−Assignment of Spectral Lines. Figure 3 shows the experimental Q-band ^{1}H ENDOR spectra of benzosemiquinone radicals in 2-propanol deuterated at different positions prepared by different methods (described below). These spectra were recorded at the magnetic field position corresponding to g_z (see Figure 2). At g_z, an essentially single-crystal-type spectrum is obtained due to orientation selection of molecules with their *z*-axis (perpendicular to the quinone plane) along the external field $\mathbf{B}_0$ (see Figure 5, B_{11}). Thus, one pair of ENDOR lines is observed for each proton (see eq 2). These ENDOR lines are centered around the ^{1}H

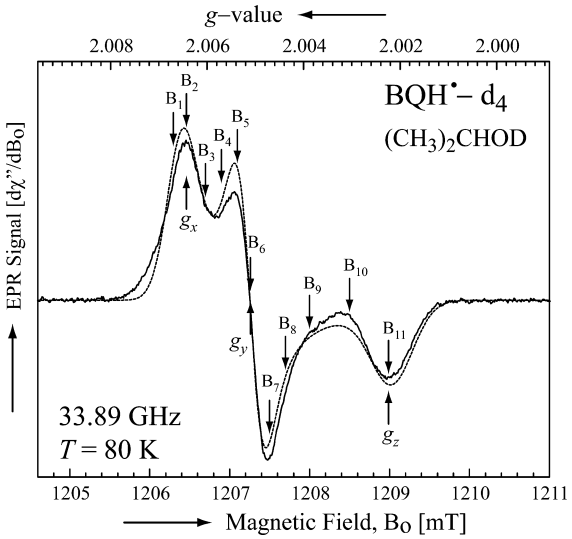

Figure 2. Experimental (solid line) and simulated (dotted line) Q-band EPR powder spectra of $BQH^{\bullet}$-d_4 in $(CH_3)_2CHOD$. ENDOR spectra were taken at the magnetic field positions indicated by arrows including those corresponding to g_x, g_y, and g_z. The line width values of ΔB_x, ΔB_y, and ΔB_z obtained from the simulation are 0.46, 0.36, and 0.61 mT. Experimental conditions: T = 80 K, microwave (MW) frequency = 33.9 GHz, spectrum obtained by pseudomodulating the field-swept FID-detected EPR spectrum with 0.15 mT, 1 scan, and 76 s per scan.

Table 1. Parameters Used in the Fittings of ^{1}H ENDOR Spectra of $BQH^{\bullet}$-d_4 in $(CH_3)_2CHOD$ at 34 GHz and T = 80 K

g-value (±0.0001)	*x*	*y*	*z*
	2.0066	2.0051	2.0022
hyperfine value[a] (MHz)	$A_{x'}$	$A_{y'}$	$A_{z'}$
O−H proton	−10.9 ± 0.1	−14.2 ± 0.1	6.5 ± 0.2
Euler angles between *A* and *g* (deg)	ϕ	θ	ψ
O−H proton	−56 ± 2	91 ± 1	10 ± 4

[a]The values obtained from the fitting correspond to the total hfc tensor components (see eq 3).

Larmor frequency (ν_{Free}) and are split by their respective hyperfine coupling A_z.

Figure 3a shows the ENDOR spectrum of a benzosemiquinone radical prepared by low temperature UV illumination in fully protonated solvent $(CH_3)_2CHOH$. The spectrum shows the line pairs L_1/L_1', L_2/L_2', L_3/L_3', and L_4/L_4' associated with hyperfine couplings of protons. For comparison, Figure 3b shows the spectrum of the anionic semiquinone prepared by reduction with alkaline solution of $(CD_3)_2CDOD$.[42,48] The spectral line labeled * is due to the ring protons 2, 3, 5, and 6 (see Figure 1) which are all equivalent in the anionic semiquinone radical. Thus, this line in the spectrum of Figure 3a is assigned to ring protons in the anionic form of the semiquinone, which obviously is generated in addition by the UV illumination but to a smaller extent than the monoprotonated semiquinone (see above).

Figure 3c shows the ENDOR spectrum of $BQD^{\bullet}$-h_4 formed by UV illumination in $(CD_3)_2CDOD$. In this ENDOR spectrum, only signals of protons from the quinone ring can be present; hence, the line pairs L_1/L_1' and L_5/L_5' are assigned

dx.doi.org/10.1021/jp304555u | J. Phys. Chem. B 2012, 116, 8890−8900

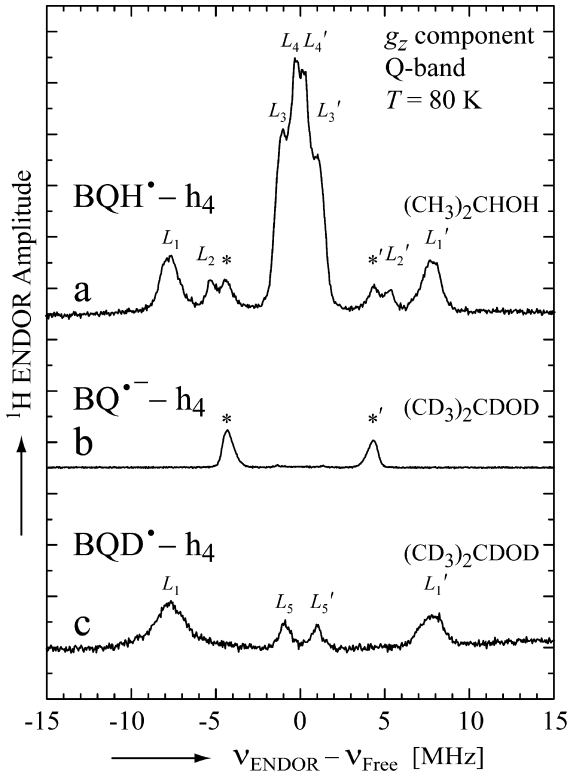

Figure 3. ^{1}H Davies Q-band ENDOR spectra of benzosemiquinone radicals prepared under different conditions. Samples were prepared: (a) by UV illumination in $(CH_3)_2CHOH$, (b) using an alkaline solution of $(CD_3)_2CDOD$ forming the anionic semiquinone radical, and (c) by UV illumination in $(CD_3)_2CDOD$. All spectra were taken along the magnetic field position corresponding to g_z (B_{11} in Figure 2), yielding single-crystal-type spectra. ENDOR lines corresponding to five different proton species are clearly observed. The respective low and high frequency peaks belonging to a hyperfine coupling are labeled (L_1/L_1', L_2/L_2', L_3/L_3', L_4/L_4', and L_5/L_5'). The lines L_2 and L_2' are assigned to the OH proton on the monoprotonated semiquinone. Experimental conditions: T = 80 K, microwave (MW) frequency = 33.9 GHz. Number of scans: 235 (a), 2093 (b), and 1885 (c). Scan time: 8 s (a), 20 s (b), and 8 s (c).

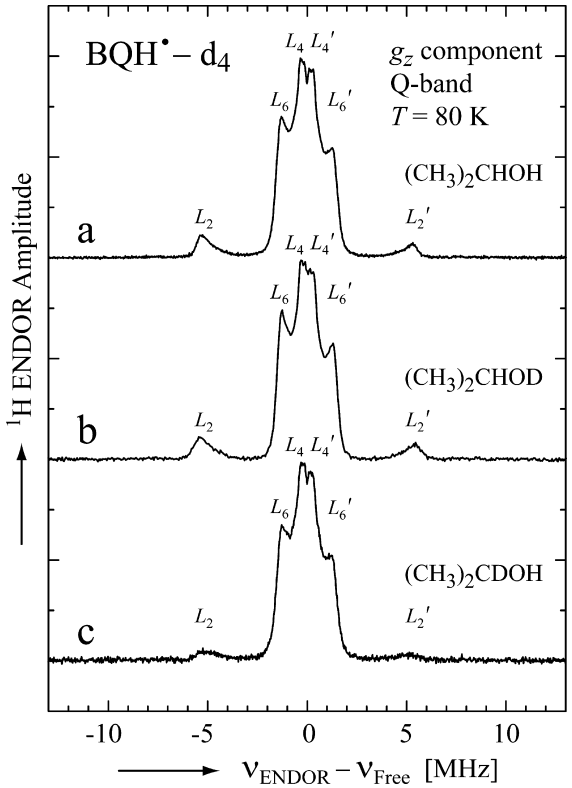

Figure 4. ^{1}H Davies Q-band ENDOR spectra of fully deuterated benzosemiquinone radicals prepared by UV illumination (BQH$^{\bullet}$-d_4) in differently deuterated 2-propanol: (a) $(CH_3)_2CHOH$, (b) $(CH_3)_2CHOD$, and (c) $(CH_3)_2CDOH$. Spectra were taken along the magnetic field position corresponding to g_z (B_{11} in Figure 2). ENDOR lines corresponding to three different proton species are clearly observed. The peaks are labeled as in Figure 3. Experimental conditions: T = 80 K, microwave (MW) frequency = 33.9 GHz. Number of scans: 55 (a), 630 (b), and 200 (c). Scan time: 103 s (a), 8 s (b), and 62 s (c).

to ring protons of the monoprotonated radical. The nonequivalence of the ring protons is due to the asymmetry in the quinone ring resulting from the protonation of only one of the oxygen atoms (O_4) of the quinone. The shift of spin density and the concomitant increase and decrease of hfc's can be qualitatively understood from the valence bond (VB) model (see Figure S2 of the Supporting Information).[71] Since the ring protons at positions 2 and 6 (see Figure 1) are expected to have a stronger hyperfine coupling than those at positions 3 and 5 (Figure 1),[28] the line pair L_1/L_1' is assigned to protons at positions 2 and 6 and the line pair L_5/L_5' is assigned to protons at positions 3 and 5. These assignments resulting from the VB model are fully supported by the DFT calculations (see below). The lines near the ^{1}H Larmor frequency in Figure 3a are due to weak interactions; i.e., L_3/L_3' and L_4/L_4' are attributed to interactions with weakly coupled solvent protons. The line pair L_2/L_2', not present in spectra 3b and 3c, corresponds to a strongly coupled proton and is assigned to the O–H proton of the neutral semiquinone radical BQH$^{\bullet}$ (see Figure 1).

Further support for this assignment of line pair L_2/L_2' to the O–H proton comes from ENDOR measurements on samples of fully deuterated benzoquinone (BQ-d_4) in differently deuterated 2-propanol, where all signals are due to protons from the solvent, including the hydroxyl proton (see Figure 4). Three solvents were studied: (a) fully protonated 2-propanol, $(CH_3)_2CHOH$; (b) 2-propanol deuterated at the hydroxyl group, $(CH_3)_2CHOD$; and (c) 2-propanol deuterated at the CH position, $(CH_3)_2CDOH$. Figure 4 shows the ENDOR spectra of all BQH$^{\bullet}$-d_4 samples taken at the field position corresponding to g_z. All lack the line labeled with an asterisk (*), supporting the assignment of this line to ring protons of the anionic semiquinone. The presence of L_2/L_2' in all spectra supports the assignment of this line pair to an interaction with a proton from the solvent. The presence of this line in $(CH_3)_2CHOD$ (Figure 4b) and its diminished intensity in $(CH_3)_2CDOH$ (Figure 4c) indicates that the proton bound to the semiquinone comes mainly from the CH group on the 2-propanol. This result supports the proposal that the mechanism for the photochemical generation of the semiquinone involves mainly hydrogen abstraction of the CH group of the 2-propanol. This mechanism leads to a stable solvent radical $(CH_3)_2C^{\bullet}OH$, which is also expected from organic radical chemistry.[29] The remains of L_2/L_2' in Figure 4c (~35%) could be due to exchange processes or other pathways. Whereas the "geometry" of the protons attached to the quinone ring of the BQH$^{\bullet}$ radical is quite straightforward (the geometry of the ring protons has been well characterized in BQ$^{\bullet-}$ (see ref 52) and

dx.doi.org/10.1021/jp304555u | J. Phys. Chem. B 2012, 116, 8890–8900

should not be affected by the monoprotonation of the semiquinone), this is not the case for the O−H proton. We have therefore performed orientation selected ENDOR experiments to determine the complete hyperfine tensor of this nucleus which are described below. Note that, despite the presence of the solvent radical in the EPR spectra, the corresponding ^{1}H ENDOR signals of the solvent radical were not observed. We attribute this to the very fast electronic relaxation (T_{1e}) of the solvent radical.

ENDOR Experiments−Orientation Selection (O−H). The geometry of the O−H proton of the molecule is an important feature of the monoprotonated semiquinone radical BQH$^\bullet$. This geometry is reflected in the hfc tensor (**A**) that describes the interaction between the unpaired electron spin and the proton. To evaluate this tensor, the magnetic field dependence of the ENDOR spectrum was determined. In order to simplify the spectrum, perdeuterated benzoquinone (d_4) was used and $(CH_3)_2CHOD$ as solvent. In this case, the only *proton* strongly bound to the semiquinone is that on the O−H group. The protons of 2-propanol, i.e., CH and CH_3, are expected to exhibit weak interactions with the unpaired electron of the neutral quinone radical, as previously shown for the anionic benzosemiquinone radical.[49,51] Since a larger spin population at O_1 is observed for the BQH$^\bullet$ radical, significant hyperfine couplings to solvent protons may occur. Figure 5 shows the experimental Q-band ^{1}H ENDOR spectra (solid lines) of BQH$^\bullet$-d_4 in $(CH_3)_2CHOD$, where the largest hfc's arise from the O−H proton. These occur at frequencies below 49.5 MHz and above 53.5 MHz. Signals of solvent (matrix) protons occur with large intensity in the central part of the ENDOR spectrum. The spectra were recorded at different magnetic fields corresponding to different positions in the EPR spectrum (see Figure 2). At the magnetic field positions from B_1 to B_9 (Figure 5), the spectra correspond to a two-dimensional powder-type spectrum with weighted contributions mainly from molecules that have the magnetic field lying in the plane of the quinone (referred to as in-plane directions). Therefore, a powder spectrum with two features, corresponding approximately to the A_x and A_y components of the hfc tensor, is observed for the O−H proton. At higher magnetic field positions (Figure 5, B_{10}−B_{11}), the ENDOR spectra arise mainly from the weighted contributions from molecules that have the magnetic field pointing perpendicular to the plane of the quinone (referred to as out-of-plane directions), and contain one rather narrow line pair stemming from the O−H proton tensor. These lines corresponding to the O−H proton are centered around the ^{1}H Larmor frequency (51.6 MHz, position B_{11}) and are split by its A_z value. The ^{1}H ENDOR lines in Figures 5, B_1−B_{11} assigned to the O−H proton, partially overlap with the lines associated with the matrix protons.

Simulations of EPR and ENDOR Spectra. The simulated EPR spectrum is shown by a dotted line in Figure 2. The principal values of the *g* tensor (g_x, g_y, and g_z) were obtained from the simulation and are summarized in Table 1. The principal axes of the *g*-tensor are expected to be approximately along the quinone axes *xyz* (see Figure 1). This has been predicted by DFT calculations performed in this work (see next section). Thus, the *g*-tensor frame provides the reference system for describing the geometry of the O−H proton (see Figure 1). The individual line width values ΔB_x, ΔB_y, and ΔB_z obtained from the fitting are given in the caption of Figure 2.

The principal components of the hfc tensor **A** and the Euler angles, ϕ (in-plane angle), θ (*azimuthal* angle), and ψ,

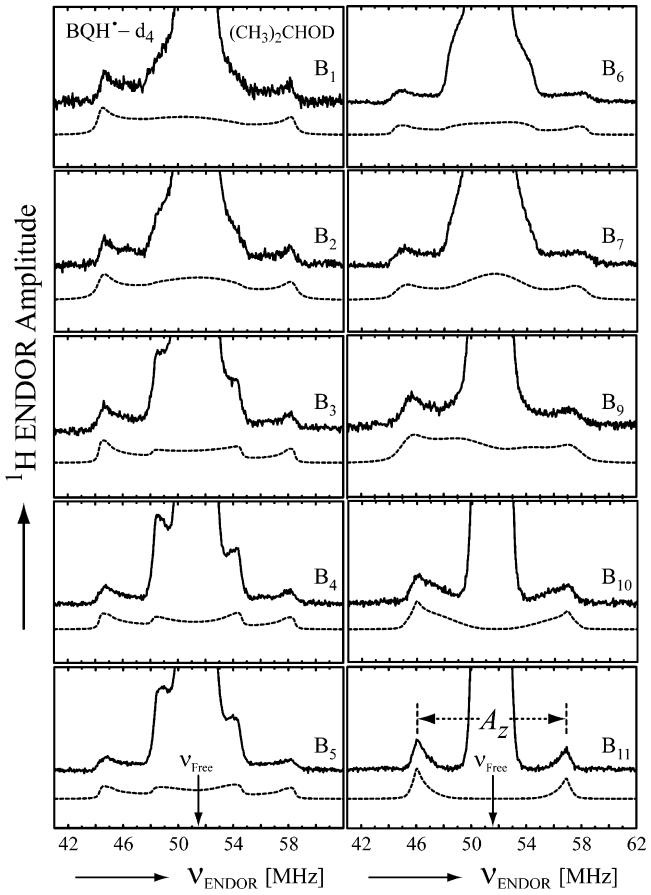

Figure 5. Experimental (solid lines) and simulated (dotted lines) ^{1}H Davies Q-band ENDOR spectra of BQH$^\bullet$-d_4 in $(CH_3)_2CHOD$ at 10 different magnetic field positions of the EPR spectrum (see arrows in Figure 2). In the fitting of the spin Hamiltonian to the data, the frequency range between 49.5 and 53.5 MHz was excluded. In addition, the smallest hfc of O−H (~6 MHz), which is clearly resolved only in the spectra recorded at magnetic fields B_3, B_4, and B_5, was fitted using the positions (frequencies) of the respective ENDOR peaks (see the Supporting Information). The hfc splitting A_z is shown by an arrow in B_{11}. Experimental conditions: T = 80 K, microwave (MW) frequency = 33.89 GHz. Number of scans per position: 420. Scan time: 8 s.

associated with rotations of the principal axes $x'y'z'$ with respect to the *g*-tensor axes *xyz* (see Figure 1), were obtained from the global fitting of the ^{1}H ENDOR spectra of BQH$^\bullet$-d_4 in $(CH_3)_2CHOD$ (see Figure 5). The values obtained at the minimum σ_G are summarized in Table 1. As expected, a hfc tensor with rhombic symmetry was deduced for the O−H proton. The signs of the ^{1}H hfc's were obtained from DFT calculations performed in this work (vide infra). The values obtained show that the principal axis associated with the smallest hfc lies in the quinone plane and along the direction where the lone pair orbital of the oxygen is expected (see Figure 1). Assuming that the principal axes of the *g*-tensor are approximately along the quinone axes *xyz* and that the smallest hfc is along the O−H bond, we deduced that the O−H bond in BQH$^\bullet$ is an in-plane bond along the direction of the lone pair orbital of the oxygen. A very similar result has also been obtained from theoretical calculations performed in this work (vide infra). Furthermore, the value obtained for ϕ (56°) and ψ (10°) shows that the principal axes of the hfc tensor of O−H are not collinear with the *g*-tensor axes of BQH$^\bullet$. The

dx.doi.org/10.1021/jp304555u | J. Phys. Chem. B 2012, 116, 8890−8900

Table 2. Comparison of Calculated and Measured Magnetic Properties (g-Tensor, ^{1}H hfc Tensors, and π Spin Populations) of Monoprotonated Benzosemiquinone ($BQH^\bullet$) in Solution[a]

species	position		theory (DFT) zero 2-propanol	theory (DFT) three 2-propanol	theory (DFT) four 2-propanol	experiment
		g_x	2.0081	2.0066	2.0065	2.0066
		g_y	2.0052	2.0050	2.0051	2.0051
		g_z	2.0022	2.0022	2.0022	2.0022
O−H proton[b]		$A'_{x'}$ (MHz)	−4.8	−4.9	−5.0	−4.7 ± 0.1
		$A'_{y'}$	−7.9	−7.9	−8.2	−8.0 ± 0.1
		$A'_{z'}$	+12.7	+12.8	+13.2	+12.7 ± 0.2
		A_{iso}	−7.9	−8.0	−7.9	−6.2 ± 0.1
		ϕ (deg)	−43	−45	−50	−56 ± 2
		θ	90	90	91	91 ± 1
		ψ	1	1	0	10 ± 4
		r_{O-H} (Å)	0.97	0.97	1.01	c
ring protons[d]	2 and 6	A_{iso} (MHz)	−16.2	−15.2	−14.0	−14.0 ± 0.1
	3 and 5	A_{iso}	+3.4	+2.6	+1.5	+2.1 ± 0.2
π spin populations[e]	O_1	ρ^π	+0.344	+0.324	+0.312	
	O_4	ρ^π	+0.092	+0.095	+0.112	
	C_4	ρ^π	+0.294	+0.297	+0.282	
	C_1	ρ^π	+0.008	+0.045	+0.057	
	C_2	ρ^π	+0.229	+0.193	+0.176	
	C_3	ρ^π	−0.079	−0.066	−0.050	
	C_5	ρ^π	−0.077	−0.070	−0.052	
	C_6	ρ^π	+0.210	+0.208	+0.189	

[a]Theoretical values were calculated considering a surrounding with ε = 20.18 (see Materials and Methods). [b]The anisotropic and isotropic contributions to the hfc tensor were calculated separately using DFT. The experimental values of the two contributions were obtained using the hf components shown in Table 1 and eq 3. [c]The length of the O−H bond can only be determined via theoretical calculations, e.g., DFT. [d]Experimental values were obtained using the hfc's measured at magnetic field positions corresponding to g_x, g_y, and g_z and eq 3. For 2 and 6, A_x = −19.7 MHz, A_y = −6.7 MHz, and A_z = −15.6 MHz, and for 3 and 5, A_x = +1.2 MHz, A_y = +3.3 MHz, and A_z = +1.9 MHz. [e]Mulliken population analysis. Experimental data are not available.

uncertainties of the values of the fitting parameters (see Table 1) were estimated from the sensitivities of σ_G to these parameters (as discussed in ref 48). The simulated spectra calculated with the optimum values of the parameters are shown in Figure 5 (dotted lines).

Density Functional Theory (DFT) Calculations. DFT calculations were performed on the monoprotonated benzosemiquinone radical ($BQH^\bullet$) with zero, three, or four additional 2-propanol molecules coordinated, i.e., hydrogen bonded, to the radical. Geometric and magnetic parameters are summarized in Table 2. Figure 6 shows the respective fully optimized geometries with three alcohol molecules forming H-bonds to the quinone oxygens and the O−H proton of the $BQH^\bullet$ forming a H-bond to the oxygen of a fourth alcohol molecule. Figure 6 also shows the SOMO and the calculated spin density distribution of $BQH^\bullet$. The problem has been studied previously using extended Hückel theory and an external electric field instead of solvent molecules.[72]

The DFT calculations performed in this work indicated that the principal directions of the g-tensor slightly deviate from the quinone molecular axes xyz. The smallest component (2.0022) points almost perpendicular to the quinone plane, i.e., almost parallel to the molecular axis z (2°), whereas the other two components lie almost in the quinone plane but are slightly rotated (11°) with respect to the molecular axes x and y (see Table S1 of the Supporting Information). Such a rotation of the in-plane axes of the g-tensor could be associated with the protonation of the quinone, since DFT calculations on the benzosemiquinone radical anion showed a negligible deviation for the in-plane axes (<1°). Due to the small deviation, we can consider the principal directions of the g-tensor to be approximately parallel to the molecular axes of the quinone also for $BQH^\bullet$.

Geometrically, the O−H proton was found to lie in the quinone plane and approximately along the direction of the lone pair orbital of the oxygen (see Figure 6). Optimal O−H bond lengths of 0.97, 0.97, and 1.01 Å were calculated for the case of zero, three, and four 2-propanol molecules, respectively (see Table 2), demonstrating a slight elongation of this bond when the O−H proton is hydrogen bonded to a solvent molecule. The smallest hfc component is parallel to the O−H bond, in agreement with our experimental findings (see Table 2). From the calculations, the largest hfc component was found to lie also in the quinone plane (ψ = 0°, see Table 2) perpendicular to the direction of the lone pair orbital of the oxygen (see Figure 1b). The experimentally determined value ψ = 10° is slightly different from that theoretically obtained for zero, three, or four 2-propanol molecules coordinated to $BQH^\bullet$. Calculations including hydrogen bonding to protons in a second coordination shell and solvent molecules above and below the quinone plane could account for some of the small deviations between the theoretical and experimental values of the geometry parameters. In addition, the conditions under which the radical was generated, i.e., low temperature (T = 77 K) illumination, prevent to a certain extent the molecules in the sample to fully relax, resulting in a solute−solvent arrangement which could be slightly different from the one obtained by DFT (fully optimized).

By using model systems with zero, three, and four alcohol molecules, the influence of hydrogen bonding on the EPR

dx.doi.org/10.1021/jp304555u | J. Phys. Chem. B 2012, 116, 8890−8900

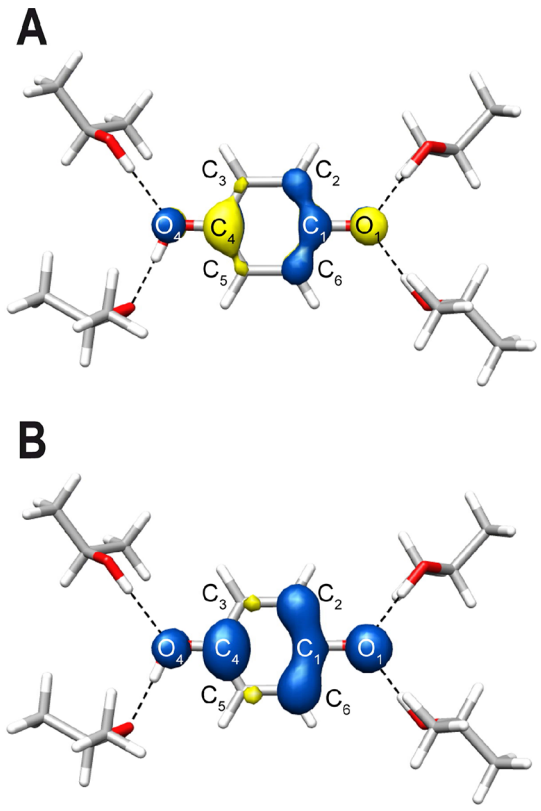

Figure 6. Presentation of the single occupied molecular orbital (SOMO) (A) and the spin density distribution of the monoprotonated benzosemiquinone radical $BQH^{\bullet}$ (B) coordinated by four 2-propanol molecules (oxygen = red, carbon = gray, hydrogen = white). The nonprotonated carbonyl oxygen (O_1, right) is hydrogen bonded to two 2-propanol molecules, and the protonated carbonyl oxygen (O_4, left), to only one 2-propanol molecule. Furthermore, the O−H proton is hydrogen bonded to the oxygen of a fourth 2-propanol molecule. In all calculations, in-plane hydrogen bonding was found.

parameters was investigated (Table 2). A detailed comparison of our results with the experimental values showed that especially the calculated values of the g_x component and the isotropic hfc (A_{iso}) of the ring protons depend strongly on the number of coordinated alcohol molecules; the agreement between theory and experiment is improved when proceeding from zero alcohol molecules to three and four alcohol molecules (see Table 2). The best agreement was obtained when four 2-propanol molecules and an additional dielectric constant of 20.18 were used in the calculations to fully mimic the solvent surrounding (the isotropic hfc's of the ring protons previously calculated by Spanget-Larsen (ref 72) agree well with those obtained in this work). These findings are in line with similar DFT studies on the benzosemiquinone radical anion, in which a larger number of solvent molecules also resulted in better agreement with the experiment, mainly for the g-tensor.[41,42] Consistently, the calculations also showed a clear influence of the hydrogen bonded alcohols on the π spin populations (see Table 2). In the present study, both the fourth alcohol molecule hydrogen bonded to the O−H proton and the more realistic dielectric constant of 20.18 seem to be relevant for obtaining a correct g-tensor.

In contrast to the trends described above, the calculated anisotropic and isotropic hfc's of the O−H proton showed no significant dependence on the number of coordinated alcohol molecules. Similar hfc's were obtained with zero and three 2-propanol molecules, indicating that the magnetic properties of the O−H proton are determined by its local surrounding (i.e., by the O−H fragment). These characteristics resemble those observed for normal α protons.[50,73] The calculated anisotropic hfc's corresponding to zero and three alcohol molecules are in excellent agreement with the experimental values, and also the calculated A_{iso} are in reasonable agreement with the experimental ones. (In the work of Spanget-Larsen (ref 72), the calculated isotropic hfc of the hydroxyl proton was remarkably overestimated. Here, the DFT approach shows better results, even when solvent molecules are not explicitly considered.) The effect of the fourth alcohol molecule on the calculated hyperfine tensor components of the O−H proton was not dramatic; however, the values obtained for the anisotropic interaction are somewhat larger than the experimental ones. This small discrepancy may be due to the limitation of our model as discussed above.

CONCLUSION

EPR and ENDOR spectroscopies at 34 GHz (Q-band) and 80 K were used to study the neutral monoprotonated 1,4-benzosemiquinone radical ($BQH^{\bullet}$) produced by illumination of the quinone in 2-propanol at cryogenic temperatures. The electronic g-tensor of $BQH^{\bullet}$ and the hyperfine coupling tensor components of protons covalently bound to $BQH^{\bullet}$ were resolved. The g-tensor of $BQH^{\bullet}$ (g_x = 2.0066, g_y = 2.0051, g_z = 2.0022) was found to be similar to the one of $BQ^{\bullet-}$ in frozen solution (g_x = 2.0065, g_y = 2.0053, g_z = 2.0023).[48,52] The signals present in the ^{1}H ENDOR spectrum of $BQH^{\bullet}$ were identified by H/D substitution. The ENDOR spectrum showed non-equivalent couplings from the ring protons, revealing a shift of the spin density over the radical as compared to the benzosemiquinone radical anion (see Figure 7). This is a consequence of the protonation of one of the oxygen atoms.[28] However, in this particular case, the shift in spin density has almost no effect on the g values of the semiquinone. In experiments in which $BQH^{\bullet}$ is formed at room temperature, the O−H proton of the radical exchanges rapidly with solvent O−H protons, making the origin of the O−H proton difficult to determine. In this study, the formation of the radical at cryogenic temperature limits the chemical exchange of the O−H proton due to the activation energy for proton transfer. This feature allows the identification of the source of the bound O−H proton. The isotope labeling experiments showed that the hydroxyl proton (O−H) of the molecule, which is abstracted from the solvent by illumination at 77 K, comes mainly from the central CH of the 2-propanol molecule. This result provides strong support for the classical mechanism for hydrogen abstraction from isopropyl groups where the solvent radical is preferentially stabilized by two methyl groups and an OH group.[74]

From the hfc tensor orientation, i.e., Euler angles (see Table 1), the direction of the O−H bond with respect to the molecule was deduced. This corresponds approximately to the direction of the lone pair orbital of the oxygen, along which the covalent bond is expected to lie. From the magnitudes of the O−H tensor components obtained from the ^{1}H ENDOR spectra of $BQH^{\bullet}$-d_4 in $(CH_3)_2CHOD$ (Table 1) and eq 3, we calculate the anisotropic and isotropic hfc's (see Table 2). A quite large isotropic hfc (−6.2 MHz) was obtained for the O−H proton. This is in fair agreement with the value (−5.0 MHz) observed at room temperature in liquid solution.[28] The larger value observed in the present study may be due to the much lower

dx.doi.org/10.1021/jp304555u | J. Phys. Chem. B 2012, 116, 8890−8900

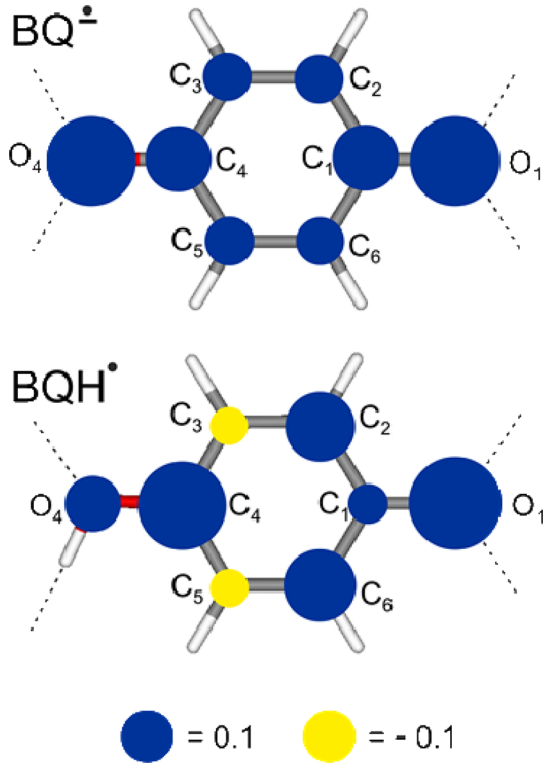

Figure 7. π-spin density distribution of the benzoquinone radical anion[42] and the monoprotonated benzosemiquinone neutral radical ligated by four 2-propanol solvent molecules (dotted lines indicate H-bonds) calculated using DFT. The spin density is proportional to the area of the circles (blue = positive, yellow = negative). For values, see Table 2 and ref 42.

temperature (80 K) by which the out-of-plane fluctuations are decreased that lead to positive coupling due to direct overlap.[75] Details of hydrogen bonding which differ in liquid solution with fast ligand exchange and frozen solution may also influence the hyperfine interaction. The large magnitude of the coupling is due to the strongly covalent character of the O−H bond, which is reflected in the short length of this bond (~1.0 Å according to the DFT calculations) and leads to a strong interaction with the unpaired electron spin that is located in the π-system of the protonated benzosemiquinone radical. The anisotropic (dipolar) hfc components (see Table 2) also reflect the strong magnetic interaction between the O−H proton and the unpaired electron spin in the quinone. The significant deviation of the O−H dipolar hyperfine tensor (components −4.7 MHz, −8 MHz, +12.7 MHz) from axial symmetry is typical for an α-proton attached to a (planar) π-system, similar to that found for a C−H fragment.[50,73] Thus, the components of the dipolar hfc tensor along with its principal directions with respect to the quinone axes show that the O−H proton (after full protonation) behaves like an aromatic α-proton. This experimental finding is in agreement with the DFT calculations performed in this work. The magnetic resonance properties and the short bond length obtained from experiment and theory, respectively, are strong indications of a covalent single bond.

The determination of the geometry and the magnetic resonance properties of the O−H proton provided a detailed picture of the geometric and electronic structure of the monoprotonated benzosemiquinone radical. The approach discussed in this paper to elucidate the geometric and electronic structure of $BQH^{\bullet}$ should be applicable to other (transient) radical species in solution and in proteins. Of particular interest is the protonated rhodosemiquinone radical ($RQ_BH^{\bullet}$) in the reaction center of *Rhodobacter sphaeroides*.[11] This species has been recently observed by EPR spectroscopy and shown to be suitable for studying the magnetic properties of the crucial high energy intermediate $Q_BH^{\bullet}$ state involved in the reduction of Q_B to Q_BH_2.[76,77] Another system in which the protonated semiquinone has been proposed is the cytochrome bo_3 ubiquinol oxidase from *Escherichia coli*.[13] However, this assignment has been questioned by MacMillan et al. who argued that the isotropic coupling calculated for the covalently bound proton was found to be larger than is observed experimentally.[14] Our experimental values show a large isotropic coupling for the covalently bound hydrogen which supports the results of MacMillan et al. Further studies of protonated semiquinone species in model systems and in proteins should help to elucidate the structural details of these important intermediates.

■ ASSOCIATED CONTENT

Ⓢ Supporting Information

A description of the simulation of the spectra, two figures showing the Q-band EPR powder spectrum of $BQH^{\bullet}$-h_4 in $(CH_3)_2CHOH$ at 77 K and a valence bond scheme to explain the spin density distribution of the neutral monoprotonated benzosemiquinone radical, a table with the g-tensor principal values and direction cosines (relative to the molecular frame), and the geometry (DFT) optimized atomic coordinates of $BQH^{\bullet}$ coordinated to 4, 3, and 0 solvent molecules (2-propanol). This material is available free of charge via the Internet at http://pubs.acs.org.

■ AUTHOR INFORMATION

Corresponding Author

*E-mail: mafloresr@asu.edu (M.F.); wolfgang.lubitz@cec.mpg.de (W.L.).

Present Addresses

[§]Department of Chemistry and Biochemistry, Arizona State University, Tempe, Arizona 85287, USA.

[∥]Chemical Sciences & Engineering, Argonne National Laboratory, Argonne, Illinois 60439, USA.

[⊥]Department of Chemistry, Pennsylvania State University, University Park, Pennsylvania 16802, USA.

Notes

The authors declare no competing financial interest.

■ ACKNOWLEDGMENTS

We thank Gudrun Klihm, Christoph Laurich, and Frank Reikowski for technical assistance and Inge Heise for the synthesis of deuterated benzoquinone (all Max Planck Institute for Chemical Energy Conversion, Mülheim an der Ruhr, Germany). This work was supported by the Max Planck Society and the EU/Energy Network project SOLAR-H2 (FP7 contract 212508). M.Y.O. thanks the National Institutes of Health (GM 41637) for support.

■ REFERENCES

(1) Trumpower, B. L. *Function of Quinones in Energy Conserving Systems*; Academic Press: New York, 1982.

(2) Lenaz, G. *Coenzyme Q: Biochemistry, Bioenergetics and Clinical Applications of Ubiquinone*; John Wiley & Sons: Suffolk, VA, 1985.

(3) Blankenship, R. E. *Molecular Mechanisms of Photosynthesis*; Blackwell Science Ltd.: Oxford, U.K., 2002.

(4) Cramer, W. A.; Knaff, D. B. In *Energy transduction in biological membranes: a textbook of bioenergetics*; Cantor, C. R., Ed.; Springer-Verlag: New York, 1990; p 193.
(5) Nohl, H.; Kozlov, A. V.; Staniek, K.; Gille, L. *Bioinorg. Chem.* **2001**, *29*, 1−13.
(6) Patai, S.; Rappoport, Z. *The Chemistry of Quinonoid Compounds*; John Wiley & Sons: Chichester, U.K.; New York, 1988.
(7) Miller, A. F.; Brudvig, G. W. *Biochim. Biophys. Acta* **1991**, *1056*, 1−18.
(8) Lubitz, W.; Feher, G. *Appl. Magn. Reson.* **1999**, *17*, 1−48.
(9) Ohnishi, T.; Johnson, J. E.; Yano, T.; LoBrutto, R.; Widger, W. R. *FEBS Lett.* **2005**, *579*, 500−506.
(10) Dikanov, S. A.; Holland, J. T.; Endeward, B.; Kolling, D. R. J.; Samoilova, R. I.; Prisner, T. F.; Crofts, A. R. *J. Biol. Chem.* **2007**, *282*, 25831−25841.
(11) Graige, M. S.; Paddock, M. L.; Feher, G.; Okamura, M. Y. *Biochemistry* **1999**, *38*, 11465−11473.
(12) Kramer, D. M.; Nitschke, W.; Cooley, J. W. In *The Purple Photosynthetic Bacteria*; Hunter, C. N., Daldal, F., Thurnauer, M. C., Beatty, J. T., Eds.; Springer Science: Dordrecht, The Netherlands, 2009; Chapter 23, pp 451−473.
(13) Yap, L. L.; Samoilova, J. I.; Gennis, R. B.; Dikanov, S. A. *J. Biol. Chem.* **2006**, *281*, 16879−16887.
(14) MacMillan, F.; Kacprzak, S.; Hellwig, P.; Grimaldi, S.; Michel, H.; Kaupp, M. *Faraday Discuss.* **2011**, *148*, 315−344.
(15) Lubitz, W.; Abresch, E. C.; Debus, R. J.; Isaacson, R. A.; Okamura, M. Y.; Feher., G. *Biochim. Biophys. Acta* **1985**, *808*, 464−469.
(16) MacMillan, F.; Lendzian, F.; Lubitz, W. *Magn. Reson. Chem.* **1995**, *33*, S81−S93.
(17) MacMillan, F.; Lendzian, F.; Renger, G.; Lubitz, W. *Biochemistry* **1995**, *34*, 8144−8156.
(18) Gardiner, A. T.; Zech, S. G.; MacMillan, F.; Käss, H.; Bittl, R.; Schlodder, E.; Lendzian, F.; Lubitz, W. *Biochemistry* **1999**, *38*, 11773−11787.
(19) Veselov, A. V.; Osborne, J. P.; Gennis, R. B.; Scholes, C. P. *Biochemistry* **2000**, *39*, 3169−3175.
(20) Grimaldi, S.; MacMillan, F.; Ostermann, T.; Ludwig, B.; Michel, H.; Prisner., T. *Biochemistry* **2001**, *40*, 1037−1043.
(21) Flores, M.; Isaacson, R.; Abresch, E.; Calvo, R.; Lubitz, W.; Feher, G. *Biophys. J.* **2006**, *90*, 3356−3362.
(22) Paddock, M. L.; Flores, M.; Isaacson, R.; Chang, C.; Abresch, E. C.; Selvaduray, P.; Okamura, M. Y. *Biochemistry* **2006**, *45*, 14032−14042.
(23) Flores, M.; Isaacson, R.; Abresch, E.; Calvo, R.; Lubitz, W.; Feher, G. *Biophys. J.* **2007**, *92*, 671−682.
(24) Paddock, M. L.; Flores, M.; Isaacson, R.; Chang, C.; Abresch, E. C.; Okamura, M. Y. *Biochemistry* **2007**, *46*, 8234−8243.
(25) Cape, J. L.; Bowman, M. K.; Kramer, D. M. *Proc. Natl. Acad. Sci. U.S.A.* **2007**, *104*, 7887−7892.
(26) Weyers, A. M.; Chatterjee, R.; Milikisiyants, S.; Lakshmi, K. V. *J. Phys. Chem. B* **2009**, *113*, 15409−15418.
(27) Bridge, N. K.; Porter, G. *Proc. R. Soc. London, Ser. A* **1958**, *244*, 259−275.
(28) Gough, T. E. *Trans. Faraday Soc.* **1966**, *62*, 2321−2326.
(29) Das, R.; Venkataraman, B. *Res. Chem. Intermed.* **2005**, *31*, 167−192.
(30) Noda, S.; Boba, T.; Mizuta, T.; Miura, M.; Yoshida, H. *J. Chem. Soc., Perkin Trans. 2* **1980**, *1*, 61−64.
(31) Hales, B. J.; Case, E. E. *Biochim. Biophys. Acta* **1981**, *637*, 291−302.
(32) Burie, J.-R.; Boussac, A.; Boullais, C.; Berger, G.; Mattioli, T.; Mioskowski, C.; Nabedryk, E.; Breton, J. *J. Phys. Chem.* **1995**, *99*, 4059−4070.
(33) Claxton, T. A.; Gough, T. E.; Symons, M. C. R. *Trans. Faraday Soc.* **1965**, *61*, 279−285.
(34) Wong, S. K.; Sytnyk, W.; Wan, J. K. S. *Can. J. Chem.* **1972**, *50*, 3052−3057.
(35) Lendzian, F.; Jaegermann, P.; Möbius, K. *Chem. Phys. Lett.* **1985**, *120*, 195−200.
(36) Rist, G. H.; Hyde, J. S. *J. Chem. Phys.* **1968**, *49*, 2449−2451.
(37) Hoffman, B. M.; DeRose, V. J.; Doan, P. E.; Gurbiel, R. J.; Houseman, A. L. P.; Telser, J. Metalloenzyme active-site structure and function through multifrequency CW and pulsed ENDOR. In *Biological Magnetic Resonance*; Berliner, L., Reuben, J., Eds.; Plenum Press: New York, 1993; Vol. *13*, pp. 151−218.
(38) Hüttermann, J. ENDOR of randomly oriented mononuclear metalloproteins: toward structural determinations of the prosthetic group. In *Biological Magnetic Resonance*; Berliner, L., Reuben, J., Eds.; Plenum Press: New York, 1993; Vol. *13*, pp. 219−252.
(39) Koch, W.; Holthausen, M. C. *A Chemist Guide to Density Functional Theory*; Wiley-VCH: Weinheim, Germany, 2001.
(40) Kaupp, M. *Calculation of NMR and EPR Parameters-Theory & Applications*; Wiley-VCH: Weinheim, Germany, 2004.
(41) Kaupp, M.; Remenyi, C.; Vaara, J.; Malkina, O. L.; Malkin, V. G. *J. Am. Chem. Soc.* **2002**, *124*, 2709−2722.
(42) Sinnecker, S.; Reijerse, E.; Neese, F.; Lubitz., W. *J. Am. Chem. Soc.* **2004**, *126*, 3280−3290.
(43) Sinnecker, S.; Flores, M.; Lubitz, W. *Phys. Chem. Chem. Phys.* **2006**, *8*, 5659−5670.
(44) Fritscher, J.; Prisner, T. F.; MacMillan, F. *Appl. Magn. Reson.* **2006**, *30*, 251−268.
(45) Niklas, J.; Epel, B.; Antonkine, M. L.; Sinnecker, S.; Pandelia, M. E.; Lubitz, W. *J. Phys. Chem. B* **2009**, *113*, 10367−10379.
(46) Weil, J. A.; Bolton, J. R.; Wertz, J. E. *Electron Paramagnetic Resonance. Elementary Theory and Practical Applications*; Wiley: New York, 1994.
(47) Weil, J. A. *J. Magn. Reson.* **1975**, *18*, 113−116.
(48) Flores, M.; Isaacson, R. A.; Calvo, R.; Feher, G.; Lubitz, W. *Chem. Phys.* **2003**, *294*, 401−413.
(49) Epel, B.; Niklas, J.; Sinnecker, S.; Zimmermann, H.; Lubitz, W. *J. Phys. Chem. B* **2006**, *110*, 11549−11560.
(50) Atherton, N. M. *Electron Spin Resonance. Theory and Applications*; Ellis Horwood: Chichester, U.K., 1973; Chapter 4, pp 134−138.
(51) O'Malley, P. J.; Babcock, G. T. *J. Am. Chem. Soc.* **1986**, *108*, 3995−4001.
(52) Burghaus, O.; Plato, M.; Rohrer, M.; Möbius, K.; MacMillan, F.; Lubitz, W. *J. Phys. Chem.* **1993**, *97*, 7639−7647.
(53) Schweiger, A.; Jeschke, G. *Principles of Pulse Electron Paramagnetic Resonance*; Oxford University Press: Oxford, U.K., 2001.
(54) Zhao, X.; Imahori, H.; Zhan, C. G.; Sakata, Y.; Iwata, S.; Kitagawa, T. *J. Phys. Chem. A* **1997**, *101*, 622−631.
(55) Reijerse, E.; Lendzian, F.; Isaacson, R.; Lubitz, W. *J. Magn. Reson.* **2012**, *214*, 237−243.
(56) Burghaus, O.; Rohrer, M.; Götzinger, T.; Plato, M.; Möbius, K. *Meas. Sci. Technol.* **1992**, *3*, 756−774.
(57) Davies, E. R. *Phys. Lett. A* **1974**, *47*, 1−2.
(58) Stoll, S.; Schweiger, A. *J. Magn. Reson.* **2006**, *178*, 42−55.
(59) Lee, C.; Yang, W.; Parr, R. G. *Phys. Rev. B* **1988**, *37*, 785−789.
(60) Becke, A. D. *J. Chem. Phys.* **1993**, *98*, 5648−5652.
(61) Stephens, P. J.; Devlin, F. J.; Chabalowski, C. F.; Frisch, M. J. *J. Phys. Chem.* **1994**, *98*, 11623−11627.
(62) Dunning, T. H. *J. Chem. Phys.* **1970**, *53*, 2823−2833.
(63) Dunning, T. H.; Hay, P. J. In *Modern Theoretical Chemistry*; Schaefer, H. F., Ed.; Plenum: New York, 1976.
(64) Neese, F. ORCA. An *ab initio*, Density Functional and Semiempirical SCF-MO Package. Version 2.9. 2012. Mülheim an der Ruhr, Germany, Max-Planck-Institut für Chemische Energiekonversion.
(65) Klamt, A. *J. Phys. Chem.* **1995**, *99*, 2224−2235.
(66) Sinnecker, S.; Rajendran, A.; Klamt, A.; Diedenhofen, M.; Neese, F. *J. Phys. Chem. A* **2006**, *110*, 2235−2245.
(67) Barone, V. In *Recent Advances in Density Functional Methods*; Chong, D. P., Ed.; World Scientific Publishing Company: Singapore, 1995.

(68) Das, R.; Radha, P. K.; Venkataraman, B. *Proc. Indian Acad. Sci. (Chem. Sci.)* **1993**, *105*, 273−277.
(69) Pedersen, J. B.; Hansen, C. E. M.; Parbo, H; Muus, L. T. *J. Chem. Phys.* **1975**, *63*, 2398−2405.
(70) Willson, R. L. *Trans. Faraday Soc.* **1971**, *67*, 3020−3029.
(71) Shaik, S. S.; Hiberty, P. C. *A Chemist's Guide to Valence Bond Theory*; John Wiley & Sons: Hoboken, NJ, 2008.
(72) Spanget-Larsen, J. *Chem. Phys. Lett.* **1976**, *44*, 543−546.
(73) McConnell, H. M.; Heller, C.; Cole, T.; Fessenden, R. W. *J. Am. Chem. Soc.* **1960**, *82*, 766−775.
(74) Turro, N. J. *Modern Molecular Photochemistry*; University Science Books: Sausalito, CA, 1991.
(75) Gough, T. E.; Taylor, G. A. *Can. J. Chem.* **1969**, *47*, 3717−3724.
(76) Paddock, M. L.; Flores, M.; Isaacson, R.; Shepherd, J. N.; Okamura, M. Y. *Appl. Magn. Reson.* **2010**, *37*, 39−48.
(77) Flores, M.; Isaacson, R.; Shepherd, J.; Paddock, M.; Okamura, M. *Biophys. J.* **2010**, *98*, 173a.